Supplementary Information (SI) for Journal of Materials Chemistry A.

Performance Enhancement of Triboelectric Nanogenerators and Exploration of Tactile Sensing using Electrospun PAN-MWCNT layer through Interface Manipulation

Shailendra Kumar[1], Rajesh Kumar Jha[1], Bhavesh Thakur[2], Tulip Biswas[2], Jay Krishna Anand[1], Chhotrai Soren[1], Durgesh Banswar[1], Shalini Singh[3], Sonika Singh[3], Sumit Sinha-Ray[2,4*] and Ankur Goswami[1,3*]

[1]Department of Materials Science and Engineering, Indian Institute of Technology Delhi, Hauz Khas New Delhi-110016, India

[2]Department of Textile and Fibre Engineering, Indian Institute of Technology Delhi, Hauz Khas New Delhi-110016, India

[3]School of Interdisciplinary Research, Indian Institute of Technology Delhi, Hauz Khas New Delhi-110016, India

[4]Department of Mechanical and Industrial Engineering, University of Illinois at Chicago, Chicago, IL- 60607-7022, USA

*Corresponding author (E-mail: ssinharay@textile.iitd.ac.in, agoswami@mse.iitd.ac.in)

Supporting Information

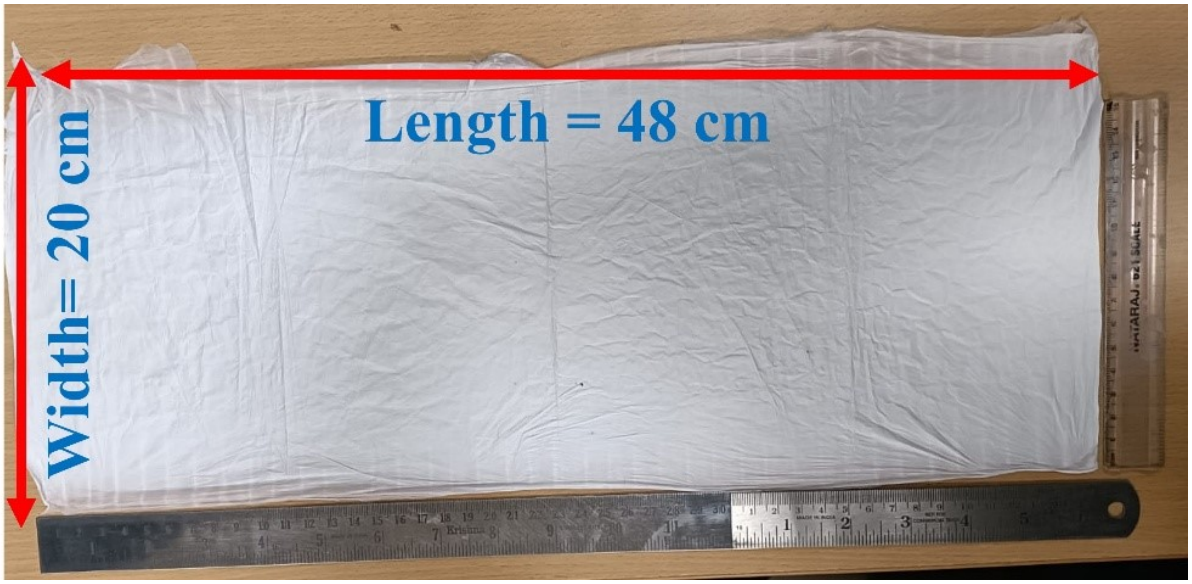

Figure S1: Large scale production of PAN-MWCNT Fiber by electrospinning process.

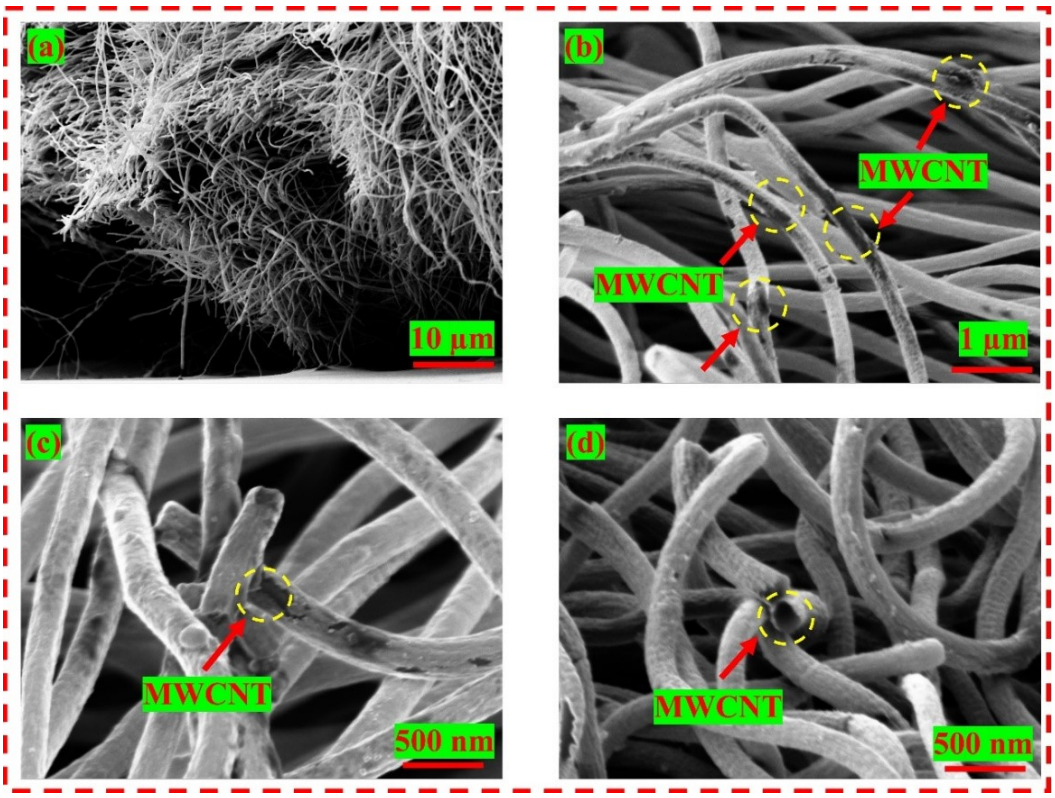

Figure S2: Cross sectional image of PAN-MWCNT nanofiber composite.

Triboelectric Nanogenerator.mp4

Video S1: In house built Triboelectric Nanogenerator (TENG) in working condition.

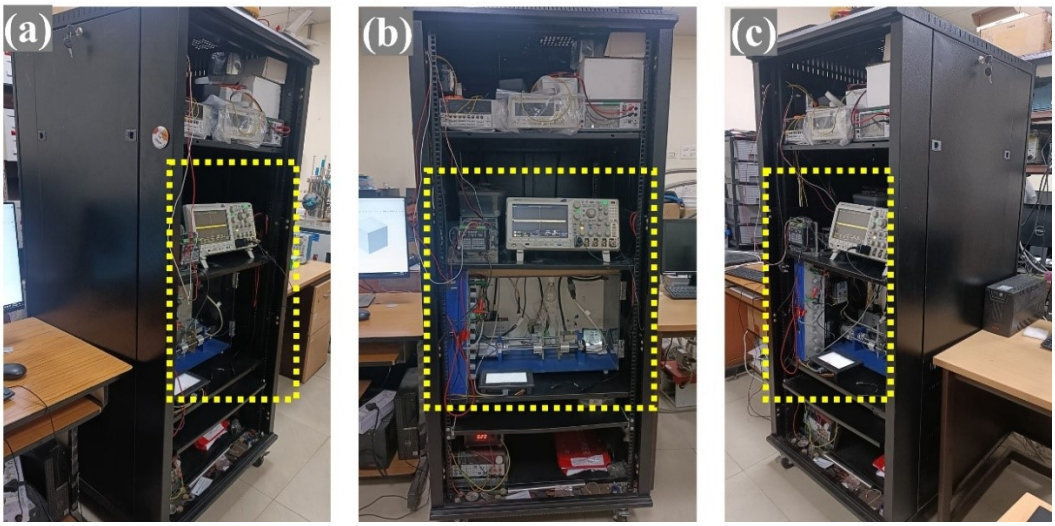

Figure S3: (a) Left side View, (b) Front View and (c) Right side View of the TENG set up place inside the metallic rack (coated with black paint) covered on three sides.

Calculation of error bar of Dielectric Constant

The dielectric constant shows a decreasing trend with increasing frequency, consistent with the expected relaxation behaviour of the materials. At lower frequency ranges, the error bars are inconsistent, indicating unstable measurements. However, as the frequency increases, a slight variation is observed, and the dielectric constant stabilizes, showing a consistent increase. The dielectric constant exhibits relatively small error margins (<4%), indicating stable performance at frequencies above 100 Hz, as depicted in Figure S4. Similarly, the standard deviation of dielectric loss and conductance across different TENG samples was calculated over five trials, revealing small error margins (<4–5%) and confirming stable performance at frequencies above the 1 kHz range.

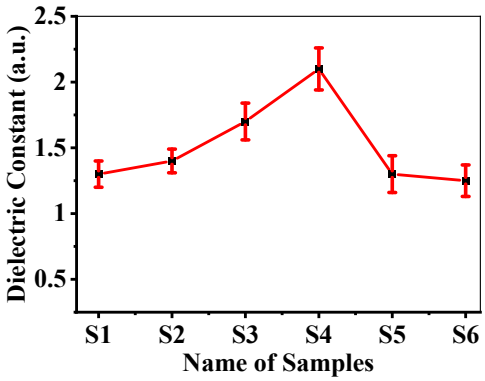

Figure S4: Error bar data for Dielectric Constant Vs Name of Samples.

Calculation of error bar open-circuit voltage (V_{OC}) and short-circuit current (I_{SC})

To evaluate the output performance of the layered TENG device, the open-circuit voltage (V_{OC}) and short-circuit current (I_{SC}) were measured for each sample (S1, S2, S3, S4, S5, and S6) at a

frequency of 2 Hz. Despite minor fluctuations in the V_{OC} and I_{SC} peaks caused by the TENG's operation, these variations could not be overlooked. Consequently, V_{OC} and I_{SC} measurements were repeated five times for each sample under identical conditions on the same setup. The voltage and current data displayed relatively small error margins (5-7%), indicating stable charge generation during repeated contact-separation cycles as shown in Figure S6 (a, and b).

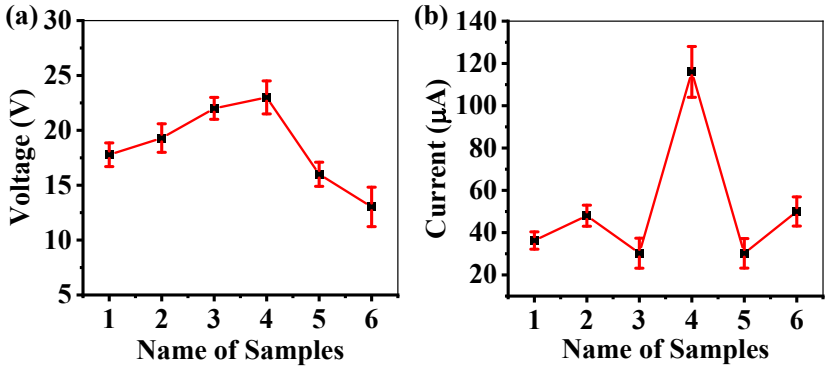

Figure S6: Error bars indicate data limitations for interpreting (a) Name of samples vs. Voltage, and (b) Name of samples vs. Current.

The standard deviation was calculated using the appropriate equation to quantify this consistency.

$$\sigma = \sqrt{\frac{1}{N-1}\sum_{i=1}^{N}(x_i - \bar{x})^2} \qquad (1)$$

Where σ is standard deviation, N-1 degree s of freedom, x_i difference between each data point, $\bar{x}$ mean and n is the total number of data points.

Subsequently, we measured the output voltage of Sample 4 under varying conditions, including different contact-separation distances between the two plates, frequencies, and applied forces. Each measurement was repeated five times per cycle, yielding relatively small error margins (5–6%). This indicates stable charge generation during repeated contact-separation cycles, as illustrated in Figure S10 (a, b, and c).

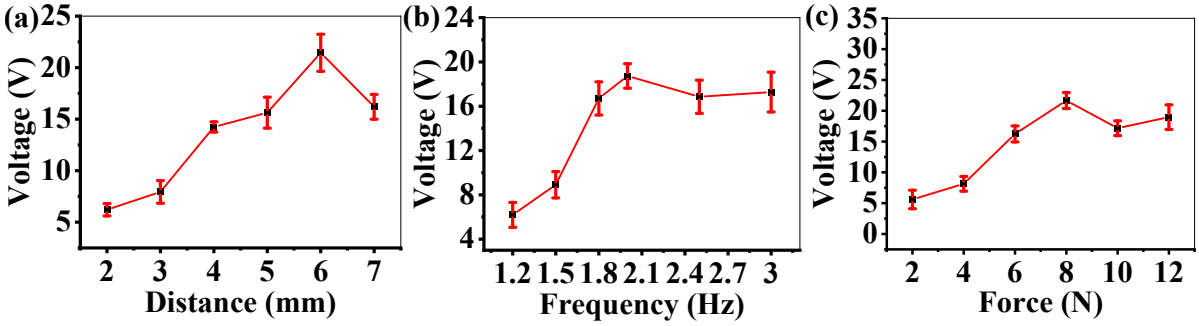

Figure S10: Error bars indicate data limitations for interpreting (a) Distance vs. Voltage, (b) Frequency vs. Voltage, and (c) Force Vs. Voltage across TENG sample 4.

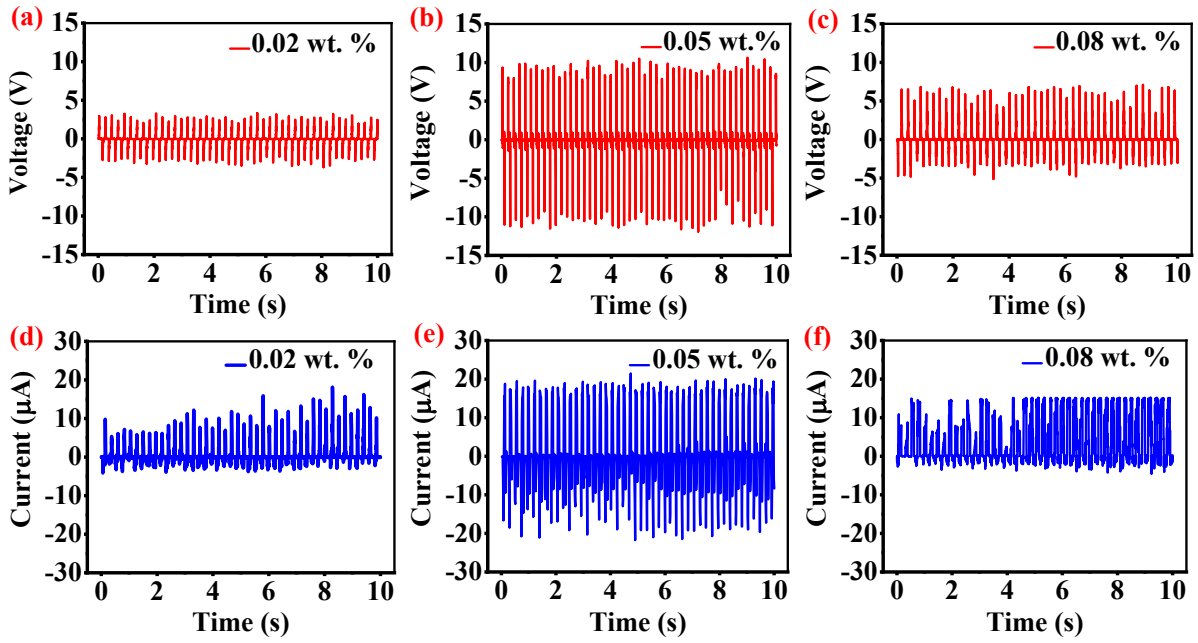

Figure S5: V_{OC} and I_{SC} for different weight percentage of Multiwall carbon nanotube (MWCNT) in PAN matrix.

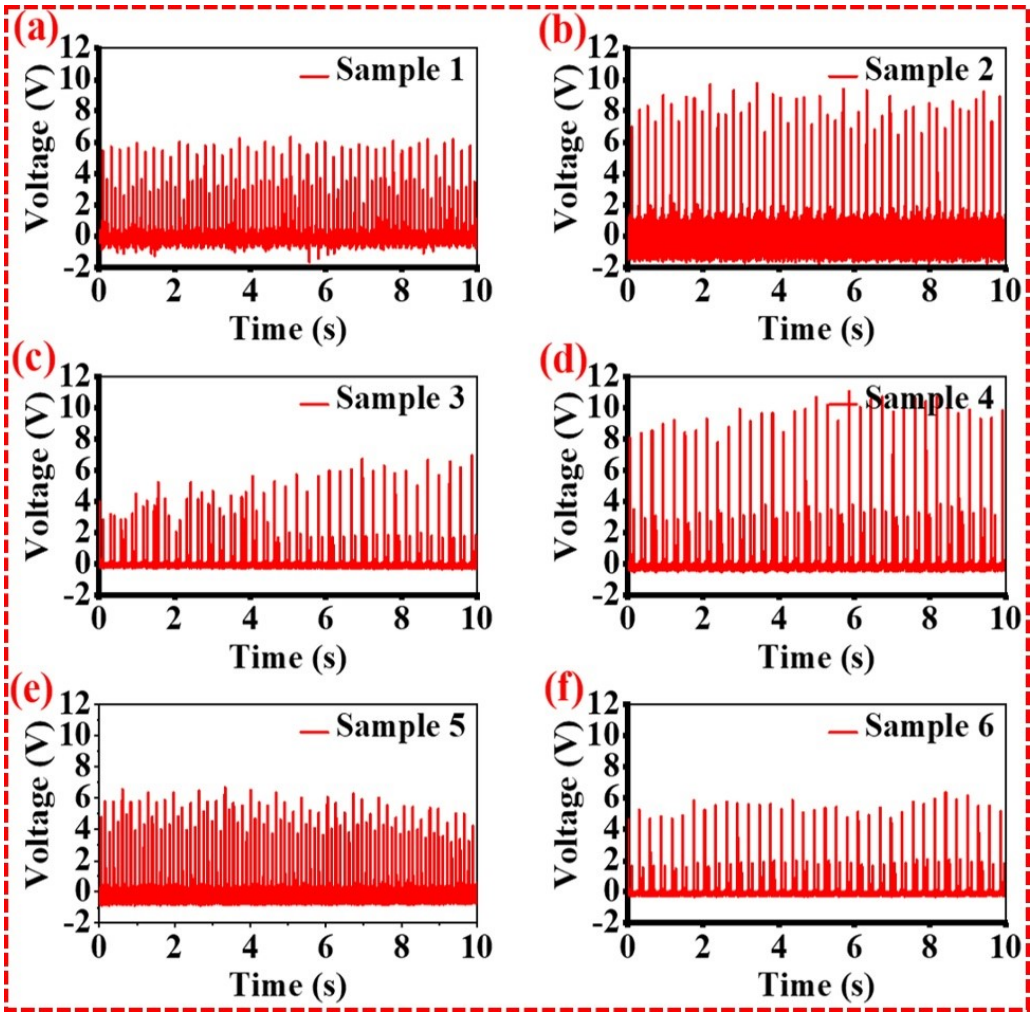

Figure S7: Rectified open circuit voltage (a-f) for different TENG samples (1,2,3,4,5,6).

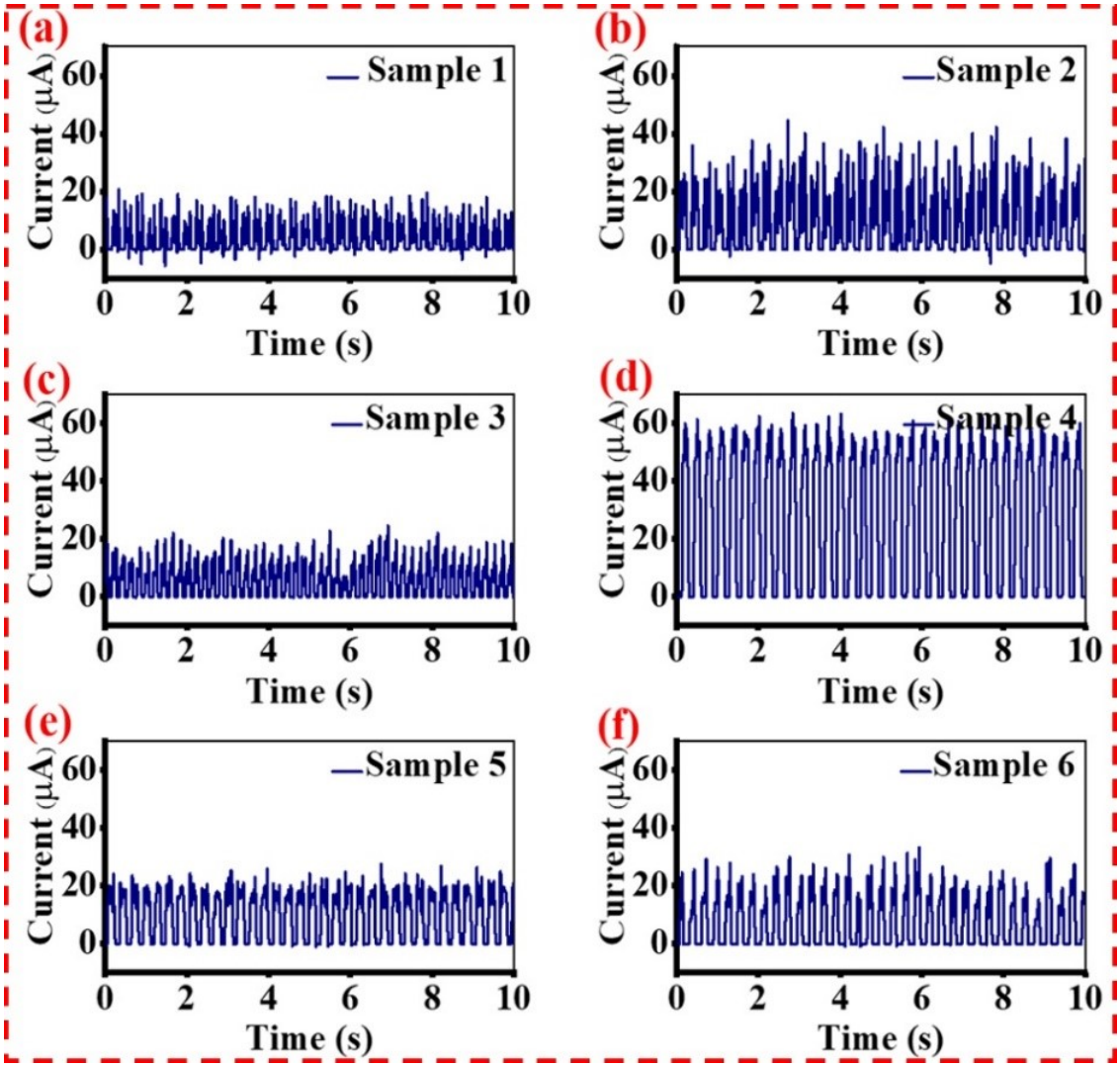

Figure S8: Rectified short circuit current (Isc) (a-f) for different TENG Samples (1,2,3,4,5,6).

Table S1: Porosity calculation of PAN and PMC nanofibers.

Sample	Sample Thickness (mm)					Avg. (mm)	Thickness of foil paper (mm)	Thickness (m)	Weight (gm)	GSM	Density (ρ) gm/cm³	Solidity	Porosity (%)
	1	2	3	4	5								
PAN	0.115	0.154	0.104	0.136	0.12	0.125	0.044	0.000081	0.0086	1.33	1.184	0.0137	98.62
PAN-MWCNT	0.247	0.264	0.244	0.218	0.26	0.246	0.044	0.00020	0.0159	2.46	1.21	0.01005	98.99

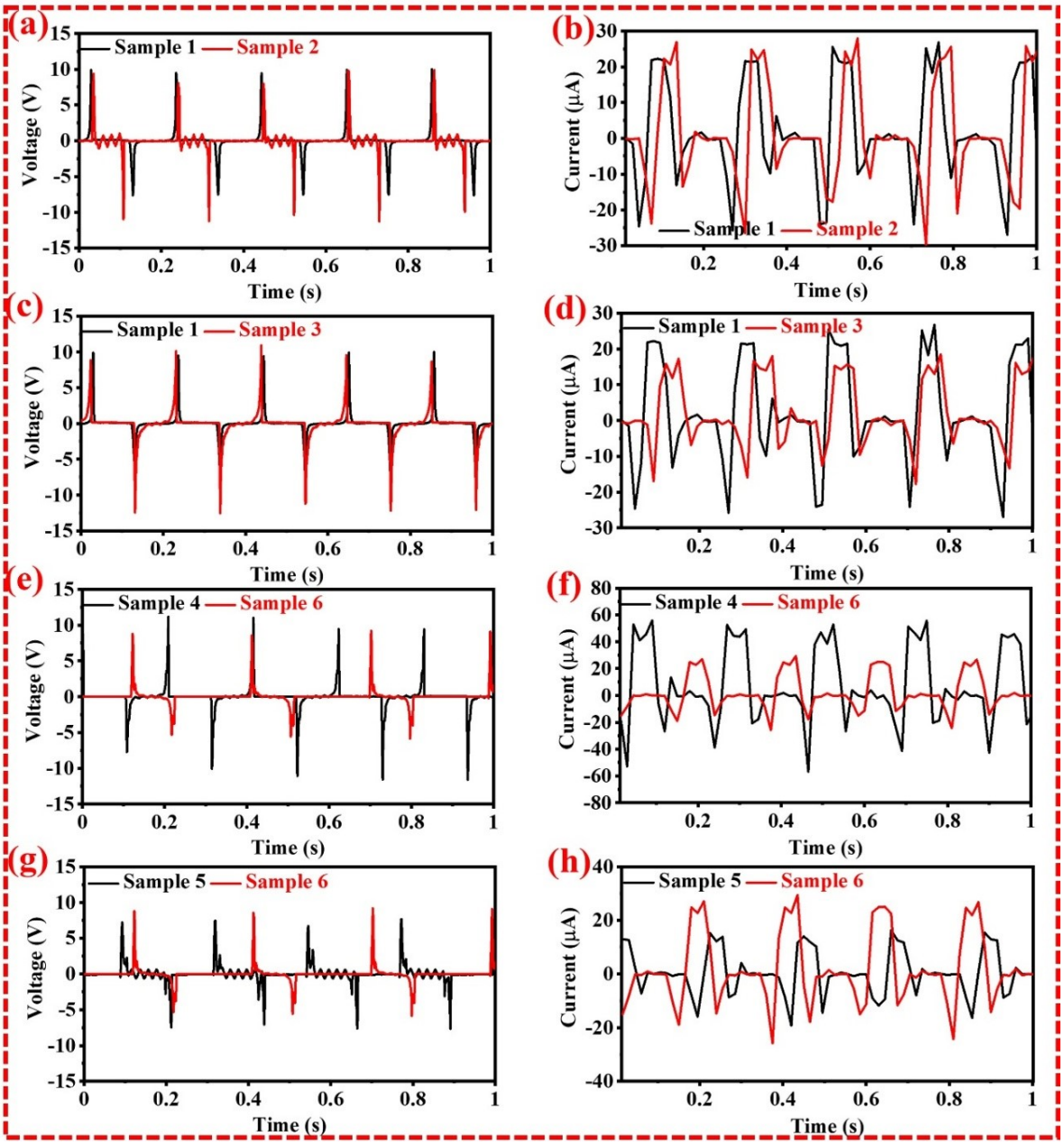

Figure S9: Enlarge the view of (a, c, e, and g) open circuit voltage and (b, d, f, and h) short circuit current of all the TENG samples.

Calculation of accumulated Charge

The accumulated charge during one half of the AC cycle:

Integrate over half a cycle t = 0 to t = T/2

$$Q_{half} = \int_0^{\frac{T}{2}} I_{max} Sin(wt) dt$$

Substitute $\omega = 2\pi f$

$$Q_{half} = \frac{I_{max}}{2\pi f}[-cos(2\pi f t)]_0^{\frac{1}{2f}}$$

$$Q_{half} = \frac{I_{max}}{2\pi f}[-(-1+1)] = \frac{2I_{max}}{2\pi f} = \frac{I_{max}}{2\pi f}$$

For Sample 1

$$Q_{full} = \frac{2I_{max} \times T}{\pi} = \frac{2 \times 19 \times 10^{-6} \times 0.06}{3.14} = 0.7\ \mu C$$

For Sample 2

$$Q_{full} = \frac{2I_{max} \times T}{\pi} = \frac{2 \times 25.5 \times 10^{-6} \times 0.06}{3.14} = 0.97\ \mu C$$

For Sample 3

$$Q_{full} = \frac{2I_{max} \times T}{\pi} = \frac{2 \times 15.5 \times 10^{-6} \times 0.06}{3.14} = 0.59\ \mu C$$

For Sample 4

$$Q_{full} = \frac{2I_{max} \times T}{\pi} = \frac{2 \times 60 \times 10^{-6} \times 0.07}{3.14} = 2.67\ \mu C$$

For Sample 5

$$Q_{full} = \frac{2I_{max} \times T}{\pi} = \frac{2 \times 16 \times 10^{-6} \times 0.05}{3.14} = 0.5\ \mu C$$

For Sample 6

$$Q_{full} = \frac{2I_{max} \times T}{\pi} = \frac{2 \times 26.5 \times 10^{-6} \times 0.07}{3.14} = 1.18\ \mu C$$

Table S2: Calculation of accumulated charge

Sample Name	Accumulated Charge (μC)
Sample 1	0.7
Sample 2	0.97
Sample 3	0.59
Sample 4	2.67

Sample 5	0.5
Sample 6	1.18

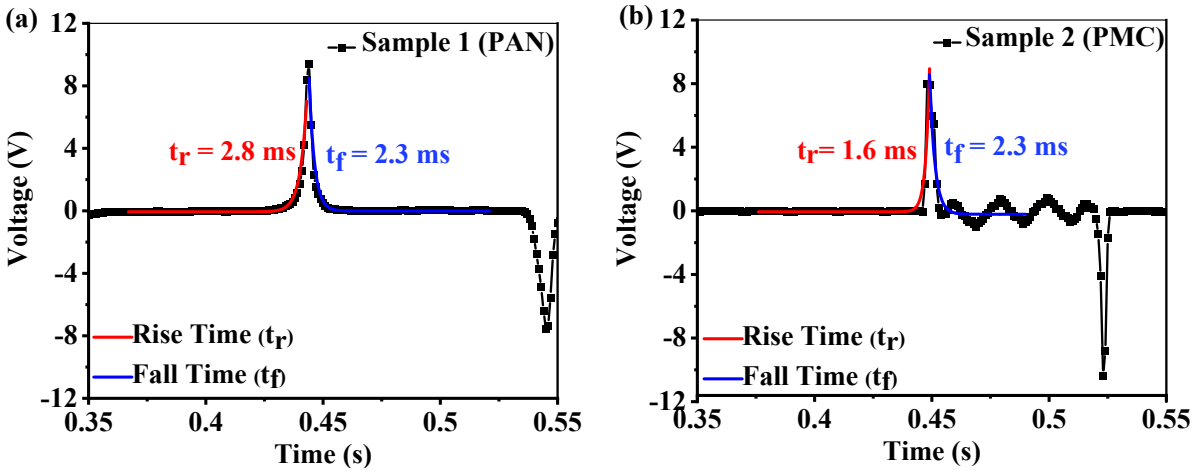

Figure S11: Lifetime of the charge carriers (a) PAN and (b) PMC nanofiber.

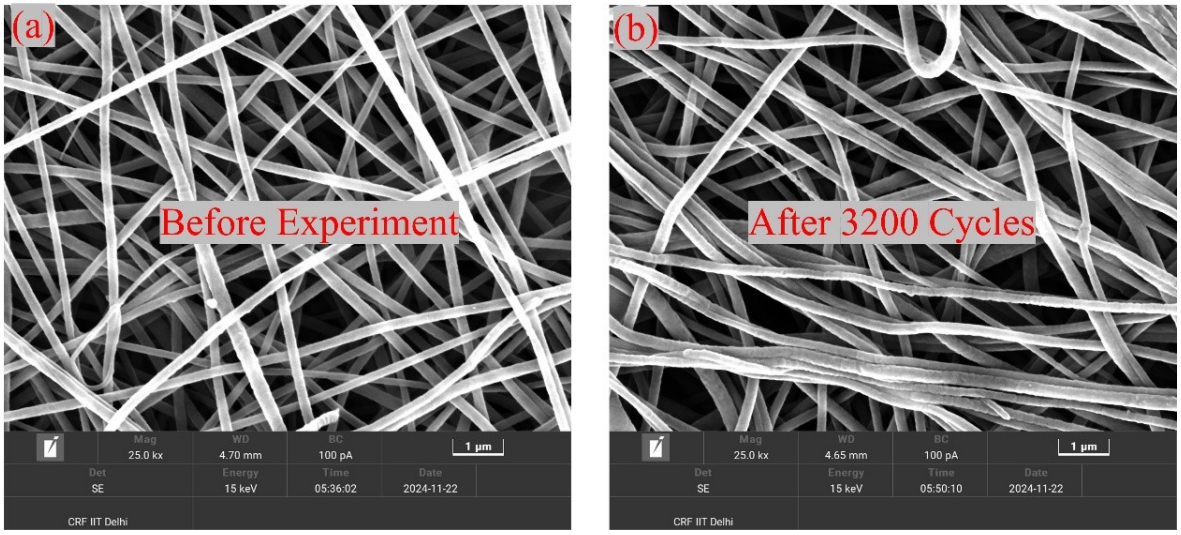

Figure S12: FESEM image of before experiment and after 3200th cycles experiment of TENG device.

Calculation to obtain σ_s, D, and E

To understand how surface charge density (σ_s) and electric flux density (D), electric field (E), and electric potential (V) are derived and related to each other, we need to delve into the foundational principles of electromagnetism and relationships between these quantities.

Derivation and Relationships

1. Surface charge Density (σ_s)

   This equation is derived from the basic definition of surface charge density. If you have a total charge Q distributed uniformly over a surface with area S, the surface charge density(σ_s) is simply the charge per unit area. This is a straightforward ratio expressing how densely the charge is packed on the surface.

2. Gauss's law in Differential Form ($\nabla.D = \rho_v$)
   Gauss's Law in its integral form is given.
   $$\oint_{\partial V} D \cdot dA = \int_V \rho_v dV \quad (1)$$
   Here, the left-hand side represents the flux of the electric displacement field D through a closed surface ∂V, and the right-hand side represents the total charge enclosed within that volume V.
   Using the divergence theorem, which states:
   $$\oint_{\partial V} D \cdot dA = \int_V (\nabla \cdot D)\, dV \quad (2)$$
   We equate the integrands to get the differential form:
   $$\nabla \cdot \mathbf{D} = \rho_v \quad (3)$$
   This equation states that the divergence of D (or known as electric flux density) at any point in space is equal to the local volumetric charge density ρ_v.

3. Electric Field from Potential ($E = -\nabla V$)
   This relationship comes from the definition of the electric potential V. The electric potential is defined as the work done per unit charge by an external force to bring a charge from infinity to a point in space. The electric field E is related to the potential by the negative gradient:
   $$E = -\nabla V \quad (4)$$
   This means the electric field points in the direction of the greatest rate of decrease of the electric potential. It indicates that if you know the spatial variation of the potential V, you can find the electric field E by taking the spatial derivative.

4. Poisson's Equation ($\nabla^2 V = -\frac{\rho_v}{\epsilon}$)
   Poisson's Equation is derived from combining Gauss's Law and the relationship between E and V. Starting from Gauss's Law in the form involving the electric field:
   $$\nabla.(\epsilon E) = \rho_v \quad (5)$$
   Substituting $E = -\nabla.V$
   $$\nabla.(\epsilon(-\nabla V)) = \rho_v \quad (6)$$
   Assuming ϵ is constant (i.e., the material is homogenous).
   $$-\epsilon \nabla.(\nabla V) = \rho_v \quad (7)$$
   Since $\nabla.(\nabla V) = \nabla^2 V$
   $$-\epsilon \nabla^2 V = \rho_v \quad (8)$$
   Or equivalently:
   $$\nabla^2 V = -\frac{\rho_V}{\epsilon} \quad (9)$$

Poisson's Equation, shows how the electric potential V is related to the charge density ρv and the permittivity of the material ϵ. It is a fundamental equation for determining the potential field generated by a given charge distribution.
The above calculation has been incorporated in supplementary section of the manuscript and highlighted the same.

COMSOL SIMULATION (Finite Element Method)

Table S3: Simulation parameters for the double-layered structure of TENG device.

S.N.	Name of Units	Units
1	Top and Bottom Electrode material	Copper
2	Top and bottom Electrode Thickness	0.1 mm
3	Top and Bottom Electrode Area	5 mm
4	Electrode dielectric constant value (ε)	1
5	Maximum Separation distance (d)	6 mm
6	Dielectric constant value of Materials ($\varepsilon_1, \varepsilon_2$)	1.1 and 1.4
7	Triboelectric Surface charge Density (σ)	5.8 x 10^{-6} C/m^2
8	Surface Area	4.0 cm^2
9	Thickness	100 µm and 150 µm

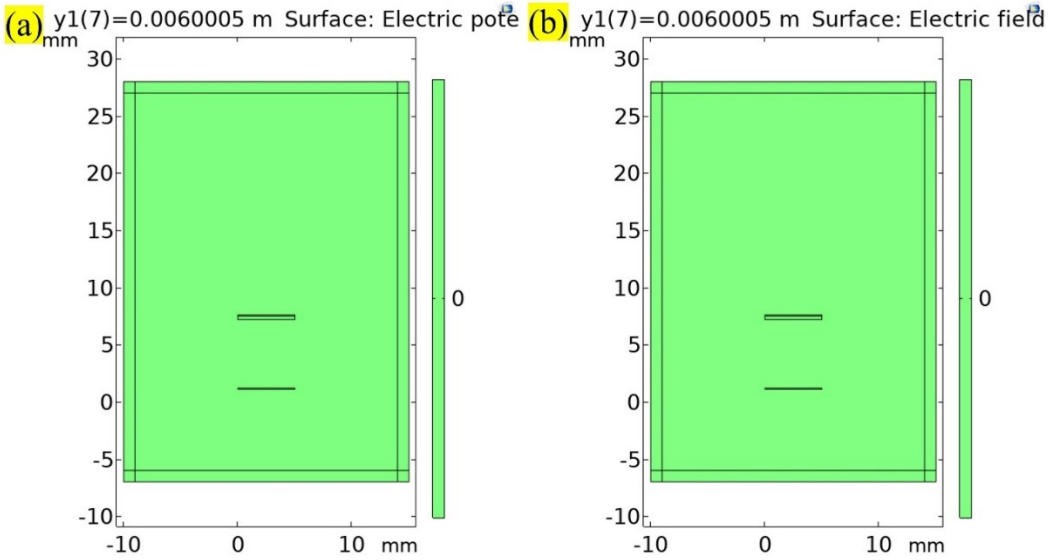

Figure S13: Surface potential and electric field distribution before initial contact.

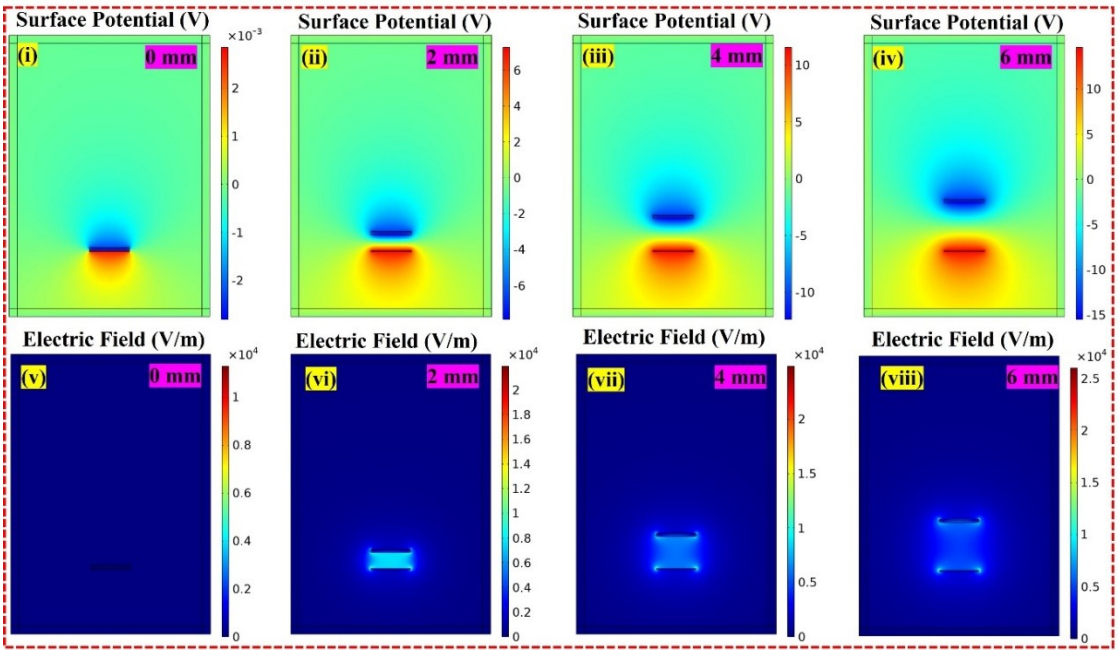

Figure S14: Electric potential distribution (i-iv) and electric field (v-viii) for contact separation mode TENG considering single layer dielectric (sample 1) thickness with 0 mm, 2 mm, 4 mm, and 6 mm distances.

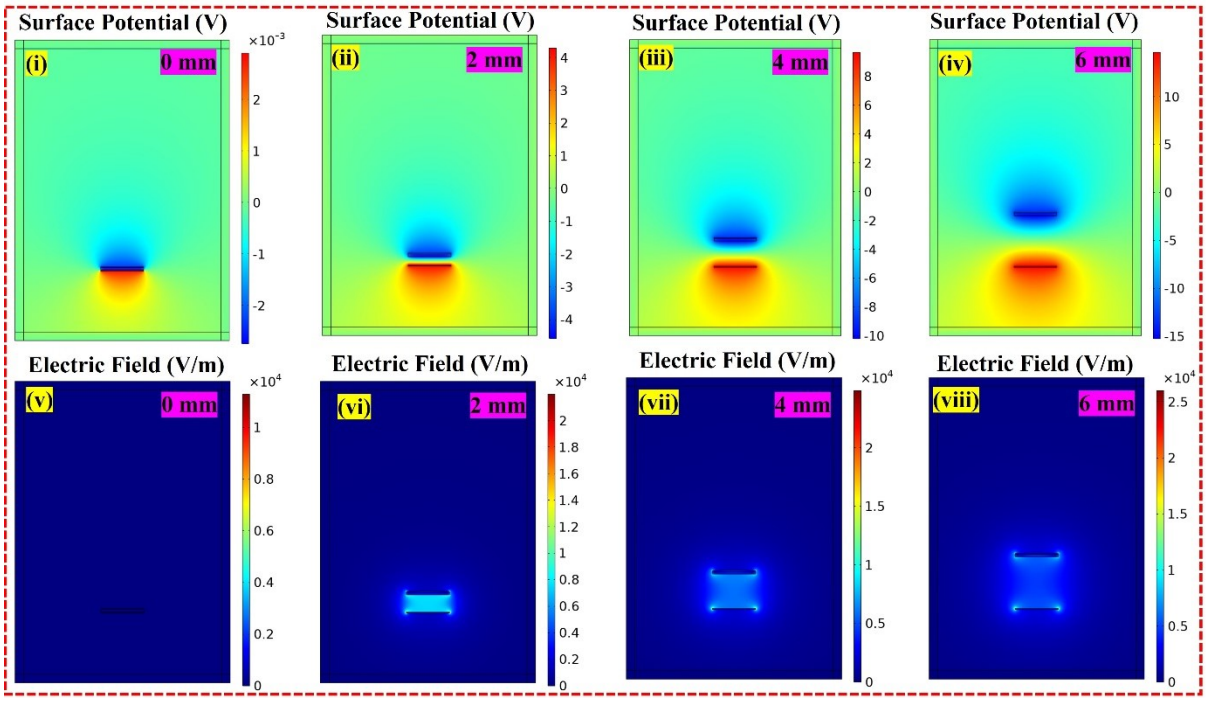

Figure S15: Electric potential distribution (i-iv) and electric field (v-viii) for contact separation mode TENG considering single layer dielectric (sample 2) thickness with 0 mm, 2 mm, 4 mm, and 6 mm distances.

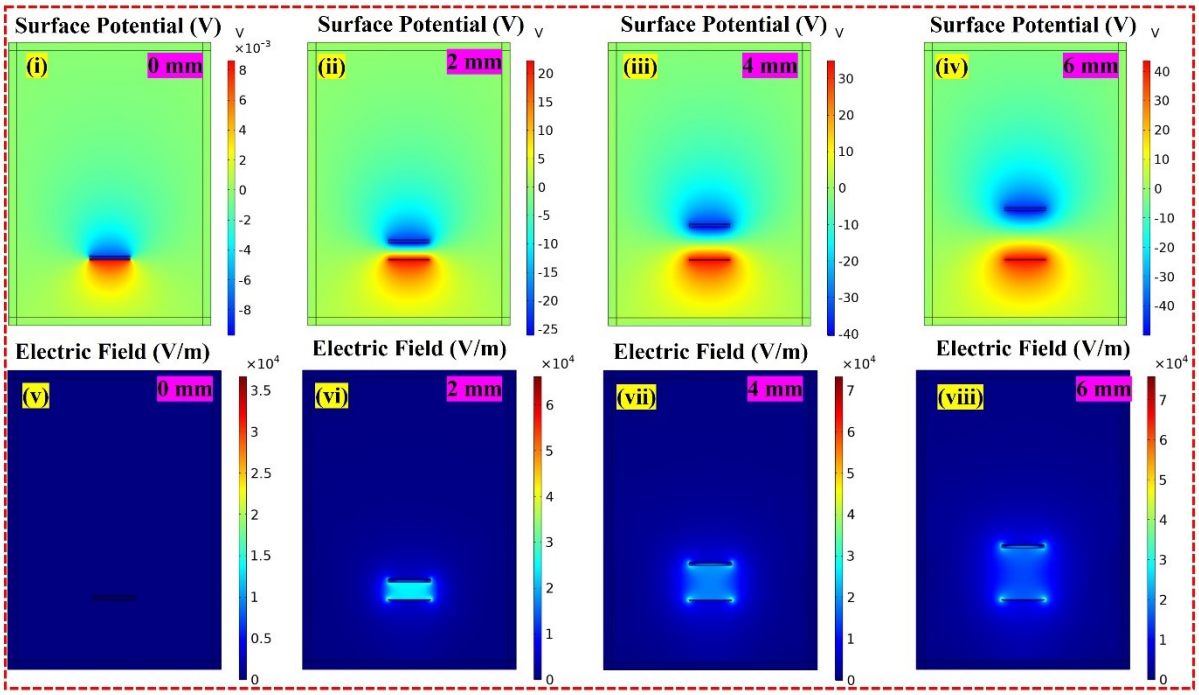

Figure S16: Electric potential distribution (i-iv) and electric field (v-viii) for contact separation mode TENG considering bi-layer dielectric (sample 3) thickness with 0 mm, 2 mm, 4 mm, and 6 mm distances.

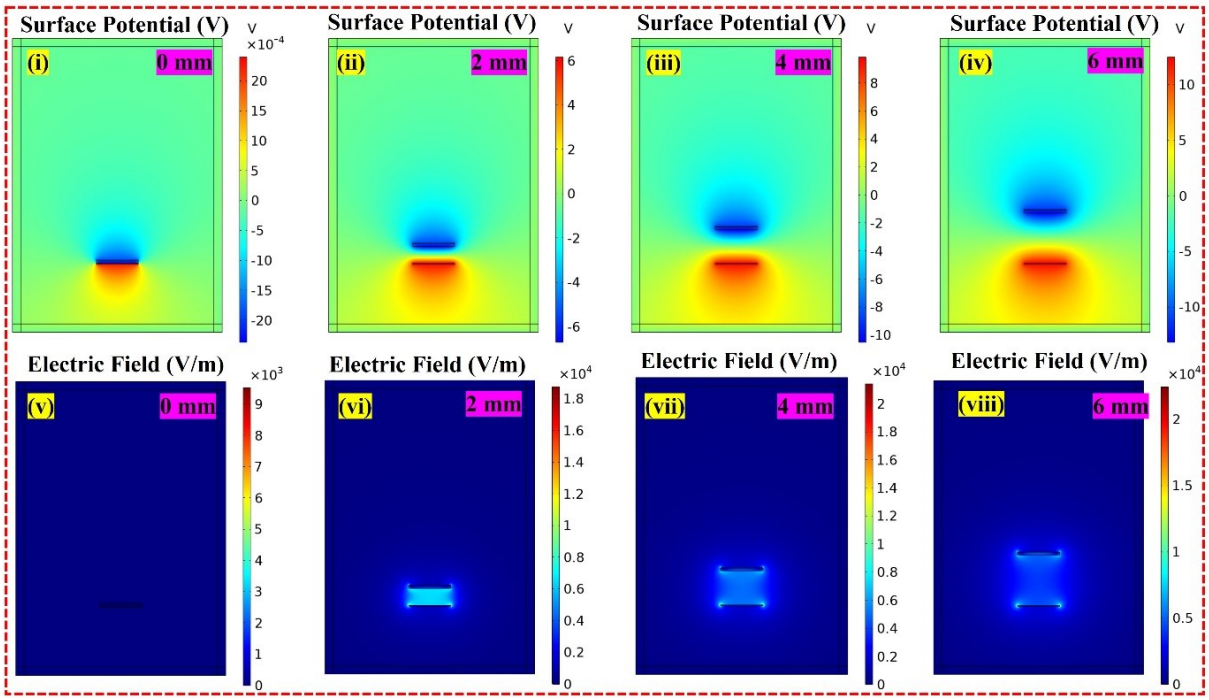

Figure S17: Electric potential distribution (i-iv) and electric field (v-viii) for contact separation mode TENG considering tri-layer dielectric (sample 5) thickness with 0 mm, 2 mm, 4 mm, and 6 mm distances.

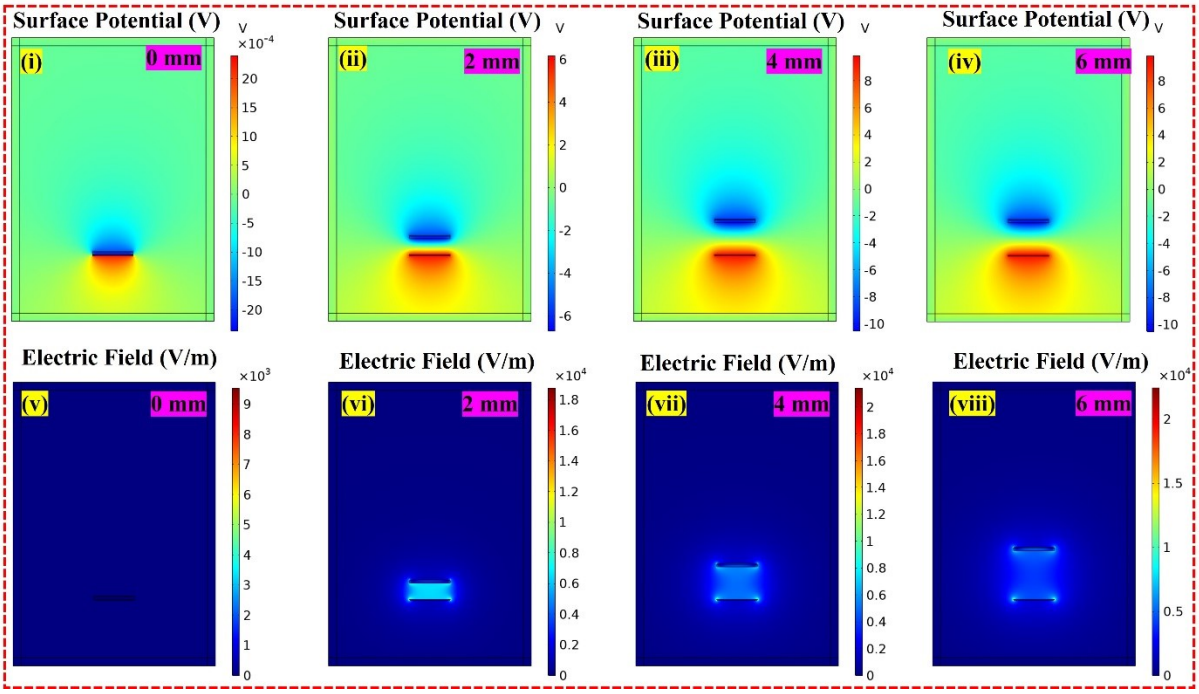

Figure S18: Electric potential distribution (i-iv) and electric field (v-viii) for contact separation mode TENG considering tri-layer dielectric (sample 6) thickness with 0 mm, 2 mm, 4 mm, and 6 mm distances.

Table S4: Surface potential and electric field distribution at different separating distances.

Distance (mm)	Sample 1		Sample 2		Sample 3		Sample 4		Sample 5		Sample 6	
	Electric Field	Electric Potential (V)	Electric Field	Electric Potential (V)	Electric Field	Electric Potential (V)	Electric Field	Electric Potential (V)	Electric Field	Electric Potential (V)	Electric Field	Electric Potential (V)
0	0.6×10⁴ V/m	0.0	0.6×10⁴ V/m	0.0	1.7×10⁴ V/m	0.0	13×10⁴ V/m	0.0	3.8×10⁴ V/m	0.0	1.7×10⁴ V/m	0.0
2	5×10⁴ kV/m	7.2	8×10⁴ kV/m	7.29	23×10⁴ kV/m	12.1	26×10⁴ kV/m	14.1	0.7×10⁴ kV/m	4.8	10×10⁴ kV/m	6.0
4	9.8×10⁴	10.2	10×10⁴ kV/m	11.4	26×10⁴ kV/m	17.9	30×10⁴ kV/m	24.1	0.8×10⁴ kV/m	9.2	12×10⁴ kV/m	9.6
6	9×10⁴	14.2	9×10⁴ kV/m	16.2	26×10⁴ kV/m	31.9	31×10⁴ kV/m	36.0	13×10⁴ kV/m	11.4	0.8×10⁴ kV/m	13.1

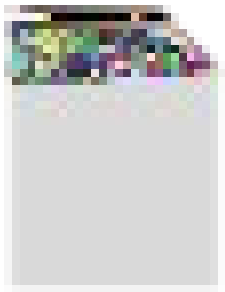

LED Glowing.mp4

Video S2: Multiple LED Glowing

Keyboard Typing.mp4

Video S3: Keyboard typing.

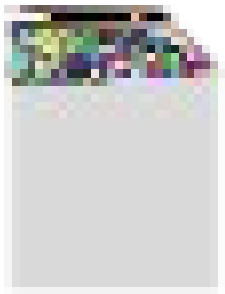

Finger Tapping.mp4

Video S4: Human Finger Tapping

Hammering.mp4

Video S5: Human Hand Hammering